CMS Physics Analysis Summary

Contact: cms-pag-conveners-exotica@cern.ch 2013/03/20

Searches for Long-lived Charged Particles in pp Collisions at $\sqrt{s} = 7$ and 8 TeV

The CMS Collaboration

Abstract

Results of searches for heavy stable charged particles produced in pp collisions at $\sqrt{s} = 7$ and 8 TeV are presented. Data collected with the CMS detector are used to study the momentum, energy deposition, and time-of-flight of candidate events. Fermions with an electric charge of $e/3$ to $5e$ as well as bound states suffering from charge flipping (charged to/from neutral) are studied. Analysis results are presented for various combinations of signatures in the inner tracker only, inner tracker plus muon system, and muon system only. Detector signatures under study are long time-of-flight to the outer muon system and anomalously high (or low) energy deposition in the inner tracker. The data are consistent with the expected background and limits on the cross section for production of long-lived scalar taus, scalar tops and gluinos, as well as direct pair production of lepton-like long-lived fermions are set.

1 Introduction

Many extensions of the standard model include heavy, long-lived, charged particles that have speed, v, less than the speed of light, c, [1–3] and/or charge, Q, not equal to $\pm 1e$ [4–7]. With lifetimes greater than a few nanoseconds, these particles can travel distances larger than the typical collider detector and appear stable (in analogy to the pion or kaon). These particles can be generically referred to as heavy stable charged particles (HSCPs) and can be singly charged ($|Q| = 1e$), fractionally charged ($|Q| < 1e$), or multiply charged ($|Q| > 1e$). Without dedicated searches, HSCPs may be mis-identified or unobserved as particle identification algorithms at hadron collider experiments generally assume signatures from standard model (SM) particles, e.g. speed very nearly equal to the speed of light and a charge of 0, or $\pm 1e$. Additionally, HSCPs may be charged during only part of their passage through detectors, further limiting the ability of standard algorithms to identify them.

For HSCP masses greater than $\gtrsim 100$ GeV/c^2, a significant fraction of particles produced at the Large Hadron Collider (LHC) will have velocity, $\beta \equiv v/c$, less than 0.9. It is possible to distinguish $|Q| \geq 1e$ particles with $\beta < 0.9$ or low momentum $|Q| < 1e$ particles from speed-of-light SM particles through their higher rate of energy loss via ionization (dE/dx) and/or through their longer time-of-flight (TOF) to the outer detectors. High momentum $|Q| < 1e$ particles are distinguishable through their lower dE/dx in comparison to SM particles.

The dependence of dE/dx on particle momentum is described by the Bethe-Bloch formula [8]. This dependence can be seen in Fig. 1 which shows dE/dx versus momentum for tracks from data and simulated HSCP signals with various charges. In the momentum range of interest at the LHC (10–1000 GeV/c), SM particles interact with nearly flat ionization energy loss ($\approx$ 3 MeV/cm). Searching for candidates with larger dE/dx gives sensitivity to massive particles with $|Q| = 1e$, particles with $|Q| > 1e$, and low momentum particles with $|Q| < 1e$. On the other hand, searching for candidates with lower dE/dx yields sensitivity to high momentum particles with $|Q| < 1e$.

Previous collider searches for HSCPs have been performed at LEP [9–12], HERA [13], the Tevatron [14–17], and the LHC [18–25]. The results from such searches have placed important bounds on beyond the standard model (BSM) theories [26, 27] such as lower limits at 95% confidence level on the mass of gluinos, scalar top quarks and pair produced scalar tau at 1098, 737 and 223 GeV/c^2, respectively. Presented here are several searches for singly, fractionally, and multiply charged HSCPs in data collected with the Compact Muon Solenoid (CMS) detector for the complete 2011 ($\sqrt{s} = 7$ TeV, 5.0 fb^{-1}) and 2012 ($\sqrt{s} = 8$ TeV, 18.8 fb^{-1}) runs.

2 Signal Benchmarks

The searches presented here are sensitive to a wide variety of signals of new, charged, massive particles. Several BSM models are used to benchmark the sensitivity. HSCPs can be categorized into two types: *lepton-like* or *hadron-like*. Lepton-like HSCPs interact primarily through the electromagnetic force while hadron-like HSCPs additionally interact through the strong force and form bound states with SM quarks (or gluons) called R-hadrons. R-hadrons can be charged or neutral. Strong interactions between the SM quarks and detector material increase energy loss and can lead to charge exchange, e.g. converting charged R-hadrons into neutral ones (and vice-versa). There is some uncertainty in the modeling of R-hadron strong interactions with detector material. For this work, two separate models are considered: (1) the model described in Ref. [28, 29], referred to as the cloud model; and (2) a model in which any strong interaction results in a neutral R-hadron [30], referred to as charge suppressed. The latter model results in

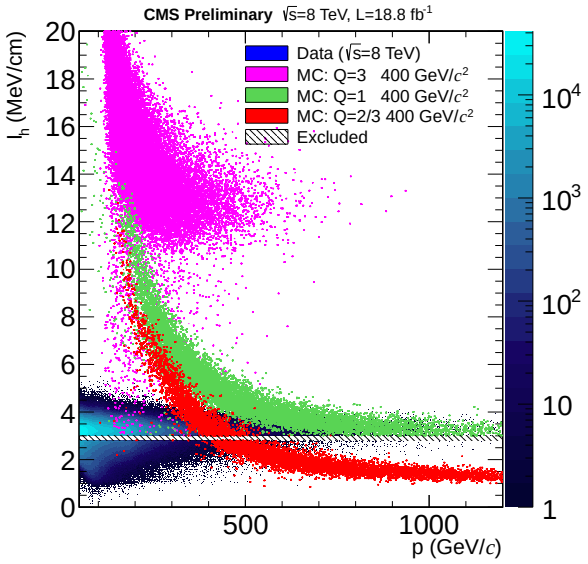

Figure 1: Distribution of dE/dx, I_h which is defined in section 3.1, versus particle momentum for data and singly, fractionally, and multiply charged HSCP candidates.

essentially all R-hadrons being neutral by the time they enter the muon system. Particle interactions with the CMS apparatus and detector response are simulated using GEANT4 v9.2 [31, 32]. To simulate the effect of multiple interactions per bunch crossing (pile-up), simulated minimum bias events are overlaid with the primary collision to match the distribution from data. The CTEQ6L1 parton distribution function (PDF) [33] is used for the sample generation.

The minimal gauge-mediated supersymmetry breaking (GMSB) model [34] allows for a stable lightest supersymmetric particle (i.e. the gravitino) and the next-to-lightest supersymmetric particle (NLSP) to be long-lived if the mass splitting between the two states is small. Studied here is the lepton-like $\tilde{\tau}_1$ NLSP case with a lifetime greater than the time-of-flight through the CMS detector. For 2011(2012) simulation, PYTHIA v6.422(v6.426) [35] is used to model both direct pair production of $\tilde{\tau}_1$'s and production of heavier supersymmetric (SUSY) particles whose decay chains include $\tilde{\tau}_1$'s (GMSB). Using parameters as in Ref. [25], $\tilde{\tau}_1$ masses of 100–494 GeV/c^2 are generated along Snowmass Slopes and Points line 7 [36]. Production cross sections for $\tilde{\tau}_1$'s are calculated at next-to-leading order (NLO) with PROSPINO v2.1 [37].

R-hadron signals from gluino and stop pair production are studied using PYTHIA v6.442(v8.153) [35, 38] for 2011(2012) generation. Stop pair production is modeled for masses of 100–1000 GeV/c^2. For $\tilde{g}$ production, split supersymmetry [39, 40] is modeled by setting the squark masses to greater than 10 TeV/c^2 and generating $\tilde{g}$ masses of 300–1500 GeV/c^2. The fraction, f, of gluinos hadronizing into $\tilde{g}$-gluon bound states is unknown. These neutral states would not leave a track in the inner detectors. Therefore, several scenarios are considered for the singly charged analysis: $f = 0.1$, 0.5, and 1.0. Gluino and stop pair production cross sections are calculated at next-to-leading order (NLO) plus next-to-leading logarithmic (NLL) accuracy with PROSPINO v2.1 [41–48].

The last of the signal samples studied is modified Drell-Yan production of long-lived lepton-like fermions. In this scenario, new massive spin-1/2 particles have arbitrary electric charge and are neutral under $SU(3)_C$ and $SU(2)_L$, and therefore couple only to the photon and the Z boson via $U(1)$ [49]. Signal samples are simulated using PYTHIA v6.422 [35] for 2011 samples and PYTHIA v6.426 for 2012 samples. The analysis uses simulations of $|Q| = 1/3, 2/3, 1, 2, 3, 4,$

and 5e for masses of 100–600 GeV/c^2 for $|Q| < e$ and 100–1000 GeV/c^2 for the other charges.

3 CMS Detector

The central feature of CMS is a superconducting solenoid of 6 m internal diameter. Within the field volume are a silicon pixel and strip tracker, a lead tungstate crystal electromagnetic calorimeter (ECAL), and a brass/scintillator hadron calorimeter (HCAL). Muons are measured in gas-ionization detectors embedded in the steel return yoke. Extensive forward calorimetry complements the coverage provided by the barrel and endcap detectors. The inner tracker measures charged particles within the pseudorapidity range $|\eta| < 2.5$. It consists of 1440 silicon pixel and 15 148 silicon strip detector modules and is located in the 3.8 T field of the superconducting solenoid. It provides a transverse momentum (p_{T}) resolution of about 1.5% for 100 GeV/c particles. Muons are measured in the pseudorapidity range $|\eta| < 2.4$, with detection planes made using three technologies: drift tubes (DT), cathode strip chambers (CSC), and resistive plate chambers (RPC). Matching muons to tracks measured in the silicon tracker results in a transverse momentum resolution between 1 and 5%, for p_{T} values up to 1 TeV/c. The first level (L1) of the CMS trigger system, composed of custom hardware processors, uses information from the calorimeters and muon detectors to select the most interesting events in a fixed time interval of less than 3 μs. The High Level Trigger (HLT) processor farm further decreases the event rate from around 100 kHz to around 300 Hz, before data storage. A more detailed description can be found in Ref. [50].

The CMS experiment uses a right-handed coordinate system, with the origin at the nominal interaction point, the x axis pointing to the center of the LHC ring, the y axis pointing up (perpendicular to the plane of the LHC ring), and the z axis along the counterclockwise beam direction. The polar angle θ is measured from the positive z axis and the azimuthal angle in the x-y plane. The pseudorapidity is given by $\eta = -\ln[\tan(\theta/2)]$.

3.1 dE/dx Measurements

As in Ref. [23], dE/dx for a track is calculated as:

$$I_h = \left(\frac{1}{N}\sum_i c_i^k\right)^{1/k}, \tag{1}$$

where c_i is the charge per unit path length in the sensitive part of the silicon detector of the i-th track measurement and $k = 2$. I_h has units MeV/cm and is computed using only measurements from the silicon strip detectors. Two additional dE/dx discriminators, $I_{as}(I'_{as})$ are used to separate SM particles from candidates with large (small) dE/dx. I_{as} is given by:

$$I_{as} = \frac{3}{N} \times \left(\frac{1}{12N} + \sum_{i=1}^{N}\left[P_i \times \left(P_i - \frac{2i-1}{2N}\right)^2\right]\right), \tag{2}$$

where N is the number of measurements in the silicon-strip detectors, P_i is the probability for a minimum–ionizing particle (MIP) to produce a charge smaller or equal to that of the i–th measurement for the observed path length in the detector, and the sum is over the track measurements ordered in terms of increasing P_i. The I'_{as} discriminator has the same form but with P_i representing the probability for a MIP to produce a charge greater or equal to that of the i–th measurement. The I_{as} and I'_{as} estimators are computed using only silicon strip measurements.

As in Ref. [23], the mass of a $|Q| = 1e$ candidate particle can be calculated based on the relationship:

$$I_h = K\frac{m^2}{p^2} + C. \tag{3}$$

where the empirical parameters $K = 2.559 \pm 0.001\,\text{MeV cm}^{-1}\,c^2$ and $C = 2.772 \pm 0.001\,\text{MeV cm}^{-1}$ are determined from data using a sample of low-momentum protons.

3.2 Time-of-flight Measurements

The time of flight to the muon system can be used to discriminate between speed-of-light particles and slower candidates. A single δ_t measurement can be used to determine the track β^{-1} via the equation:

$$\beta^{-1} = 1 + \frac{c\delta_t}{L} \tag{4}$$

where L is the flight distance. The track β^{-1} value is calculated as the weighted average of the β^{-1} measurements from the DT and CSC systems associated with the track. The weight for the i^{th} DT measurement is given by:

$$w_i = \frac{(n-2)}{n}\frac{L_i^2}{\sigma_{DT}^2} \tag{5}$$

where n is the number of ϕ projection measurements found in the chamber from which the measurement comes and σ_{DT} is the time resolution of the DT measurements, for which the measured value of 3 ns is used. The factor $(n-2)/n$ acounts for the fact that residuals are computed using two parameters of a straight line determined from the same n measurements (minimal number of hits in a given DT chamber that allows for at least one residual calculation is $n = 3$). The weight for the i^{th} CSC measurement is given by:

$$w_i = \frac{L_i^2}{\sigma_i^2} \tag{6}$$

where σ_i, the measured time resolution, is 7.0 ns for cathode strip measurements and 8.6 ns for anode wire measurements.

The resolution on the β^{-1} measurement is approximately 0.065 in both the CSC and DT subsystems.

4 Data Selection

The analyses of HSCP candidates fall into multiple topologies. Singly charged HSCPs are searched for in three ways: (1) requiring tracks be reconstructed in both the inner silicon detectors and the muon system, referred to as the "tracker+TOF" analysis; (2) only requiring tracks be reconstructed in the inner silicon detectors, the "tracker-only" analysis; and (3) only requiring tracks be reconstructed in the muon system, the "muon-only" analysis. The latter two cases account for the possibility of charge flipping (charged to neutral or vice versa) within the calorimeter. The muon-only analysis is the first CMS result that does not require a HSCP to be charged in the inner tracker. Fractionally and multiply charged candidates are searched for using a tracker-only type and tracker+TOF type analysis respectively, but with different selection, background estimate, and systematic uncertainties. The preselection for these categories is described below.

All events are required to pass a trigger requiring either the reconstruction of a muon with high transverse momentum or the calculation of large missing transverse energy, $E_{\mathrm{T}}^{\mathrm{miss}}$, using an online particle-flow algorithm [51]. The L1 muon trigger allows for late arriving particles (such as slow moving HSCPs) by accepting tracks that produce signals in the RPCs within either the 25 ns time window corresponding to the interaction bunch crossing or the following 25 ns time window. For the data used in this analysis, the second 25 ns time window is empty of proton-proton collisions.

The $E_{\mathrm{T}}^{\mathrm{miss}}$ trigger allows for recovery of some events in which no HSCP is charged in both the inner tracker and muon subsystems. The particle-flow algorithm rejects tracks reconstructed only in the inner tracker with a track p_T much greater than the matched energy deposited in the calorimeter [52] as would be the case for HSCPs becoming neutral in the calorimeter. The algorithm also rejects tracks reconstructed only in the muon system. Thus only the energy these HSCPs deposit in the calorimeter, roughly 10-20 GeV, will be included in the $E_{\mathrm{T}}^{\mathrm{miss}}$ calculation. In events in which no HSCPs are reconstructed as muon candidates, significant $E_{\mathrm{T}}^{\mathrm{miss}}$ will result if the vector sum of the HSCPs' momenta is large.

For all the analyses, the muon trigger requires $p_{\mathrm{T}} > 40\,\mathrm{GeV}/c$ measured in the inner tracker and the $E_{\mathrm{T}}^{\mathrm{miss}}$ trigger requires $E_{\mathrm{T}}^{\mathrm{miss}} > 150\,\mathrm{GeV}$. The muon-only analysis uses the same two triggers, plus a second muon trigger that requires both $p_{\mathrm{T}} > 70\,\mathrm{GeV}/c$ (using only the muon system) and $E_{\mathrm{T}}^{\mathrm{miss}} > 55\,\mathrm{GeV}$. For the first 700 pb^{-1} of 2012 data, the requirement was $E_{\mathrm{T}}^{\mathrm{miss}} > 65\,\mathrm{GeV}$. Using multiple triggers in all the analyses allows for increased sensitivity to HSCP candidates that arrive in the muon system very late as well as for *hadron-like* HSCPs which are sometimes charged in only one of the inner tracker and muon subsystems and sometimes charged in both. The muon-only analysis uses only $\sqrt{s} = 8\,\mathrm{TeV}$ data as the necessary triggers were not available in 2011.

For the tracker-only analysis, all events are required to have a candidate track with $p_{\mathrm{T}} > 45$ GeV/c (as measured in the inner tracker), relative uncertainty on p_{T} ($\sigma_{p_{\mathrm{T}}}/p_{\mathrm{T}}$) less than 0.25, $|\eta| < 2.1$, track fit $\chi^2/d.o.f. < 5$, and magnitudes of the impact parameters d_z and d_{xy} both less than 0.5 cm (d_z and d_{xy} are the longitudinal and transverse impact parameters with respect to the primary vertex which yields the smallest $|dz|$ for the candidate track). The cuts on the impact parameters are very loose compared with the resolutions for tracks in the inner tracker. Candidates must pass isolation requirements in the tracker and calorimeter. The tracker isolation criteria is $\Sigma p_T < 50$ GeV/c where the sum is over all tracks (except the candidate) within $\Delta R = \sqrt{(\Delta\phi)^2 + (\Delta\eta)^2} < 0.3$. The calorimeter isolation criteria is $E/P < 0.3$ where E is the sum of energy deposited in the calorimeter towers within $\Delta R < 0.3$ and P is the track momentum reconstructed from the inner tracker. Candidates must have at least two measurements in the silicon pixel detector, and at least eight measurements in the strip or pixel detectors. In addition, there must be measurements in at least 80% of the silicon layers between the first and last measurements of the track. To reduce the rate of contamination from clusters with large energy deposition due to overlapping tracks, a cleaning procedure is applied to remove clusters in the silicon strip tracker that are not consistent with passage of a single charged particle (e.g. a narrow cluster with most of the energy deposited in one or two strips). After cluster cleaning, there must be at least six measurements in the silicon strip detector that are used for the dE/dx calculation. Finally, $I_h > 3.0\,\mathrm{MeV/cm}$ is required.

The tracker+TOF analysis applies the same criteria, but additionally requires a reconstructed muon matched to the track in the inner detectors. At least eight independent measurements are needed for the TOF computation. Finally, $1/\beta > 1$ and $\sigma_{1/\beta} < 0.07$ are required.

The muon-only analysis uses separate criteria that include requiring a reconstructed track in

the muon system with $p_{\mathrm{T}} > 80$ GeV/c within $|\eta| < 2.1$. The resolution on p_T is approximately 10% in the barrel region and approaching 30% for $|\eta| > 1.8$ [53]. However, charge flipping by R-hadrons can make their average charge while passing through the muon system to be less than one leading to straighter tracks and their p_T to be overestimated. The effect is more pronounced for gluinos where all of the electric charge comes from SM quarks. The candidate track must have measurements in two or more DT or CSC stations, and $|d_z|$ and $|d_{xy}| < 15$ cm (calculated using tracks from the muon system and measured from the beam spot rather than the reconstructed vertex). The cuts on $|d_z|$ and $|d_{xy}|$ are approximately 90% and 95% efficient for prompt tracks, respectively. To reject cosmic muons, candidates are removed if there is a muon segment with η within 0.1 of $-\eta_{cand}$, where η_{cand} is the η of the HSCP candidate, and with $|\delta\phi| > 0.3$. Also candidates are rejected if $70^\circ < |\phi| < 110^\circ$. To reject muons from out of time pile-up, tracks are removed if their time leaving the interaction point as measured by the muon system is within ± 5 ns of an out of time pile-up event. Finally, the same quality cuts on the $1/\beta$ measurement apply as per the tracker+TOF analysis.

The fractionally charged search uses the same preselection criteria as the tracker-only analysis except requiring $I_h < 2.8$ MeV/cm. An additional veto on cosmic muons rejects candidates with a track with $p_{\mathrm{T}} > 40$ GeV/c in the opposite side of the detector ($\Delta R < 0.3$).

The multiply charged particle search uses the same preselection as the tracker+TOF analysis except that the E/P selection is removed. Also, given that a multiply charged particle might have a cluster shape different than a $|Q| = 1e$ particle, the cluster cleaning procedure is not applied for the multiply charged analysis.

5 Background Prediction

For all the analyses, the results are based on a counting experiment in the final selection (see Sec. 7) with a data driven method used to estimate the background contribution to the signal region. Candidates passing the preselection criteria (Sec. 4) are subject to two (or three) additional criteria to further improve the signal to background ratio. By choosing criteria that are uncorrelated, it is possible to use the candidates that fail one (or more) of these criteria to predict the background with the $ABCD$ method where D, the background expectation in the signal region, is estimated by $D = BC/A$, where $B(C)$ is the number of candidates that fail the first(second) criteria but pass the other one, and A is the number of candidates that fail both criteria.

For the tracker-only analysis, the two chosen criteria are p_{T} and I_{as}. Threshold values ($p_{\mathrm{T}} > 70$ GeV/c and $I_{as} > 0.4$) are fixed such that failing candidates passing only $I_{as}(p_{\mathrm{T}})$ fall into the $B(C)$ regions. The $B(C)$ candidates are then used to form a binned probability density function in $I_h(p)$ such that, using the mass determination (Eq. 3), the full mass spectrum of the background in the signal region D can be predicted. The η distribution of candidates at low dE/dx differs from the distribution of the candidates at high dE/dx. To correct for this effect, events in the C region are weighted such that its η distribution matches that in the B region.

For the tracker+TOF analysis, three criteria are used, p_{T}, I_{as}, and $1/\beta$, creating eight regions labeled $A - H$. Final threshold values are selected to be $p_{\mathrm{T}} > 70$ GeV/c, $I_{as} > 0.125$, and $1/\beta > 1.225$. Region D represents the signal region, with events passing all three criteria. The candidates in the A, F, and G regions pass only the $1/\beta$, I_{as}, and p_{T} criteria, respectively, while the candidates in the B, C, and H regions fail only the p_{T}, I_{as}, and $1/\beta$ criteria, respectively. The E region fails all three criteria. The background estimate can be made from several different combinations of these regions. The combination $D = AGF/E^2$ is used because it yields the

smallest statistical uncertainty. Similar to the tracker-only analysis, events in the G region are reweighted to match the η distribution in the B region. From the spread in background estimates from the other combinations, a 20% systematic uncertainty is assigned to the background estimate. This is also used for the tracker-only analysis.

In order to check the background prediction, loose selection samples which would be dominated by background tracks are used for the tracker-only and tracker+TOF analyses. The loose selection sample for the tracker-only analysis is defined as $p_T > 50\,\text{GeV}/c$ and $I_{as} > 0.10$. The loose selection sample for the tracker+TOF analysis is defined as $p_T > 50\,\text{GeV}/c$, $I_{as} > 0.05$, and $1/\beta > 1.05$. Figure 2 shows the observed and predicted mass spectrum for these samples.

The muon-only analysis uses the p_T and $1/\beta$ criteria for the $ABCD$ method. The final selections are $p_\text{T} > 230$ GeV/c and $1/\beta > 1.4$. It has been found that these variables are correlated with whether the candidate is in the central ($|\eta| < 0.9$) or forward ($0.9 < |\eta| < 2.1$) region of the detector and with the number of muon stations used to fit the candidate. Therefore, the background prediction is performed in six separate bins (central/forward and 2/3/4 muon stations). The final result is computed from a sum of these six bins. The systematic uncertainty on this background estimate is determined by defining four additional regions A', B', C', and D'. Events in $B'(A')$ pass(fail) the p_T criteria, but with $0.8 < 1/\beta < 1.0$ while events in $D'(C')$ pass(fail) the p_T criteria with $1/\beta < 0.8$. Two complementary predictions now become possible, $D = CB'/A'$ and $D = CD'/C'$. From the spread of the three estimates, a systematic uncertainty of 20% is assigned to the $ABCD$ method for the muon-only analysis.

The muon-only analysis also has background contributions from cosmic muons. The number of cosmic muons expected to pass the selection criteria is determined by using the sideband region of $70 < |d_z| < 120$ cm. To increase the number of cosmic tracks in the sideband region the cosmic veto requirements are not applied in the sideband region. To reduce the contamination from muons from collisions in the sideband region the tracks are required to not be reconstructed in the inner tracker. The number, N, of tracks in the sideband with $1/\beta$ greater than the threshold is counted. To determine the ratio, R_μ, of candidates in the signal region with respect to the sideband region a pure cosmic sample is used. The pure cosmic sample is collected using a trigger requiring a track from the muon system with $p_\text{T} > 20$ GeV/c, rejecting events within ± 50 ns of a beam crossing, and rejecting events triggered as beam halo. The cosmic muon contribution to the muon-only analysis signal region is determined as $N \times R_\mu$. A similar procedure is used to subtract the estimated cosmic contribution to the A, B, and C regions prior to estimating the collision background in the D region. The systematic uncertainty on the cosmic muon contribution is determined by comparing estimates using $|d_z|$ ranges of 30–50 cm, 50–70 cm, 70–120 cm, and >120 cm. It is determined to be 80%. The cosmic muon contribution to the signal region constitutes approximately 60% of the expected background.

The number of predicted and observed events in both the control region with $1/\beta < 1$ and the signal region for various p_T and $1/\beta$ thresholds are shown in Figure 3 at $\sqrt{s} = 8$ TeV. The number of predicted events includes both the cosmic and collision contributions. Only statistical uncertainties are shown.

The multiply charged analysis uses the I_{as} and $1/\beta$ criteria. Since the default track reconstruction code assumes $|Q| = 1e$ for p_T determination, the transverse momentum for $|Q| > 1e$ particles is underestimated by a $1/|Q|$ factor. Therefore p_T is not used in the final selection. In addition, while dE/dx scales as Q^2, the dynamic range of the silicon readout reaches overflow for $\approx$3 times that of a speed-of-light $|Q| = 1e$ particle. The systematic uncertainty on the background estimate for the multiply charged analysis is determined in a similar method as for the collision muon background in the muon-only analysis. Two complementary estimates

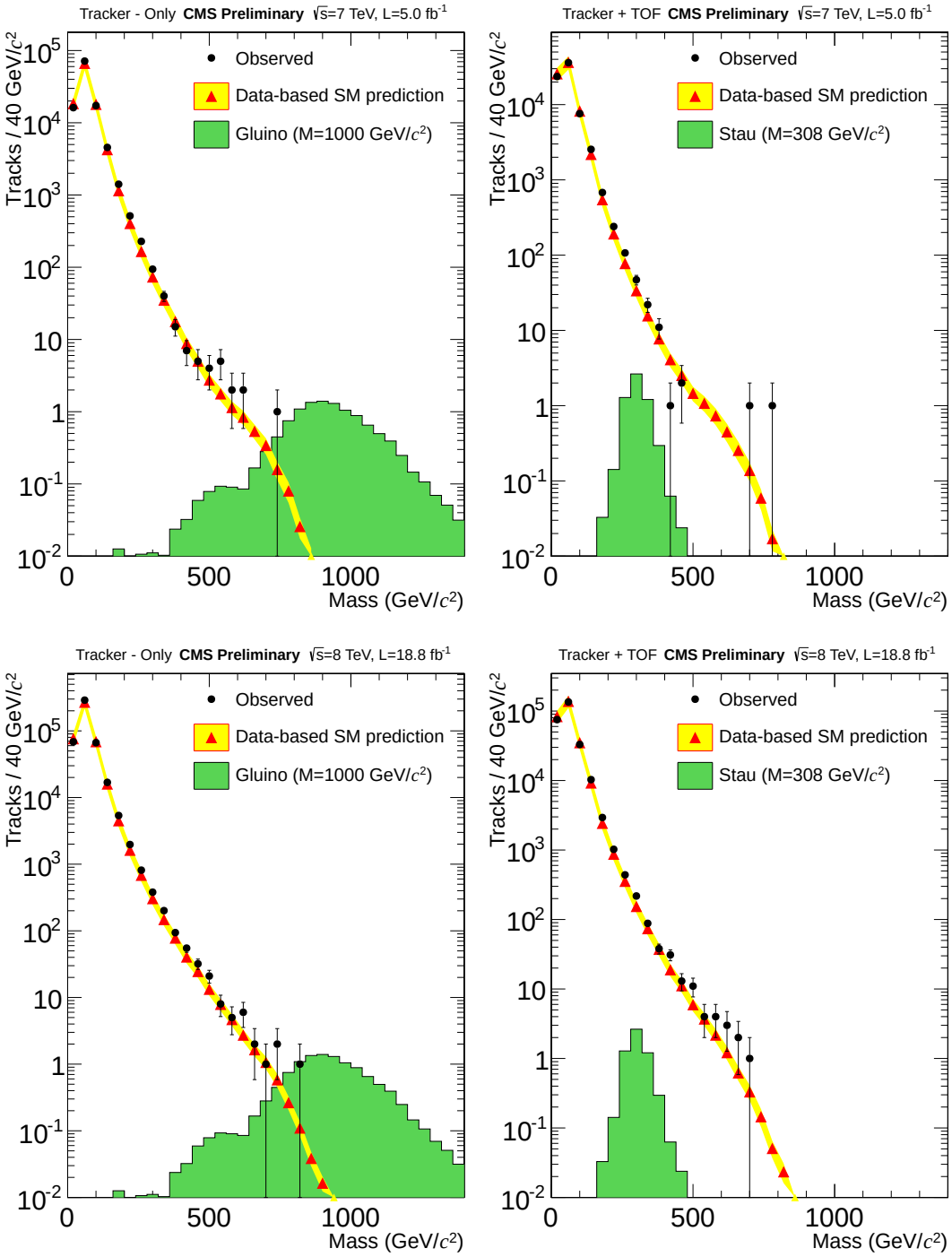

Figure 2: Observed and predicted mass spectra for candidates entering the tracker-only (left column) or tracker+TOF (right column) signal region for the loose selection. The expected distribution for a representative signal is shown in green. The top row is for $\sqrt{s} = 7\,\text{TeV}$, while the bottom row is for $\sqrt{s} = 8\,\text{TeV}$.

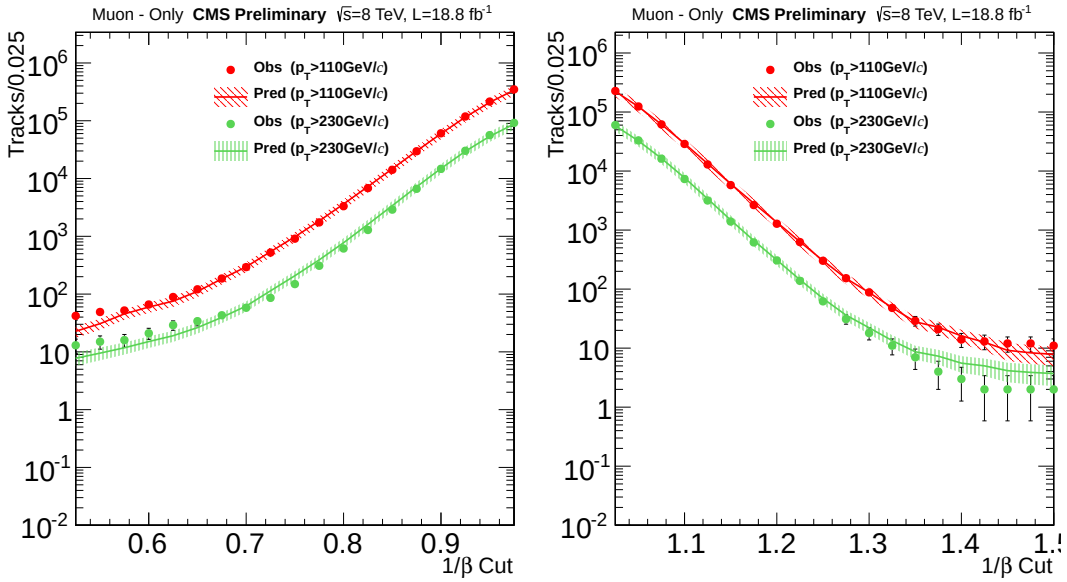

Figure 3: Observed and predicted number of tracks in both the control region with $1/\beta < 1$ (left) and the signal region (right) for two different p_T thresholds at $\sqrt{s} = 8$TeV for the muon-only analysis. The $1/\beta$ threshold is set by the X-axis. Only statistical uncertainties are shown.

from the $1/\beta < 1.0$ region are used to assess a 20% uncertainty.

Figure 4 shows the number of predicted and observed events for various I_{as} and $1/\beta$ thresholds. Uncertainties are only statistical.

The fractionally charged analysis uses the same method to estimate the background as the tracker-only analysis, replacing the I_{as} variable with I'_{as} and not applying a mass cut. The systematic uncertainty on the prediction is taken from the tracker+TOF analysis. In addition, the cosmic muon background is considered due to out-of-time cosmics often producing tracker hits with lower energy readout and late signals in the muon system. The cosmic background is found to be small and a 50% uncertainty is assigned to the prediction.

The number of predicted and observed events for various p_T and I_{as} thresholds can be seen in Figure 5. Uncertainties are only statistical.

For each analysis, fixed selections on the appropriate set of I_{as}, I'_{as}, p_{T}, and $1/\beta$ are used to define the final signal region (and the regions for the background prediction). These values are chosen to give good discovery potential over the signal mass regions of interest. For the tracker-only and tracker+TOF analyses, an additional requirement on the reconstructed mass is applied. The mass requirement depends upon the HSCP signal. For a given model and $M(HSCP)$, the mass region is $M_{reco} - 2\sigma$ to 2 TeV/c^2 where M_{reco} is the average reconstructed mass for the given mass $M(HSCP)$ and σ is the expected resolution. Simulation is used to determine M_{reco} and σ.

Table 1 lists the final selection criteria, the predicted number of background events, and the number of events observed in the signal region. Agreement between prediction and observation is seen over the full range of analyses. Figure 6 shows the observed and predicted mass distribution for the tracker-only and tracker+TOF with the tight selection.

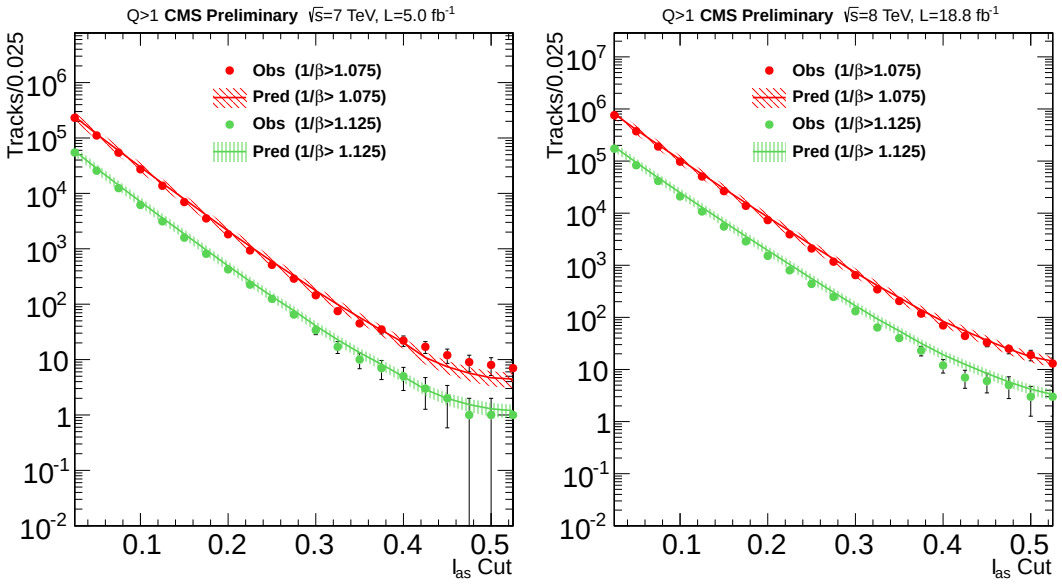

Figure 4: Observed and predicted number of tracks for two different $1/\beta$ thresholds at $\sqrt{s} = 7$ TeV (left) and 8 TeV (right) for the multiply charged analysis. The I_{as} threshold is set by the X-axis. Only statistical uncertainties are shown.

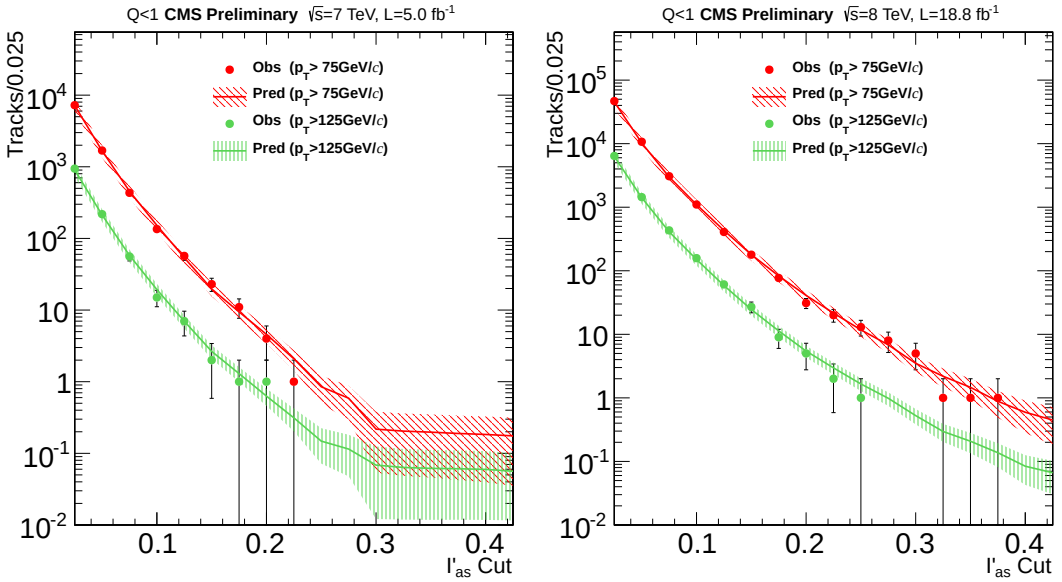

Figure 5: Observed and predicted number of tracks for two different p_T thresholds at $\sqrt{s} =$ 7TeV (left) and 8TeV (right) for the fractionally charged analysis. The I'_{as} threshold is set by the X-axis. Only statistical uncertainties are shown.

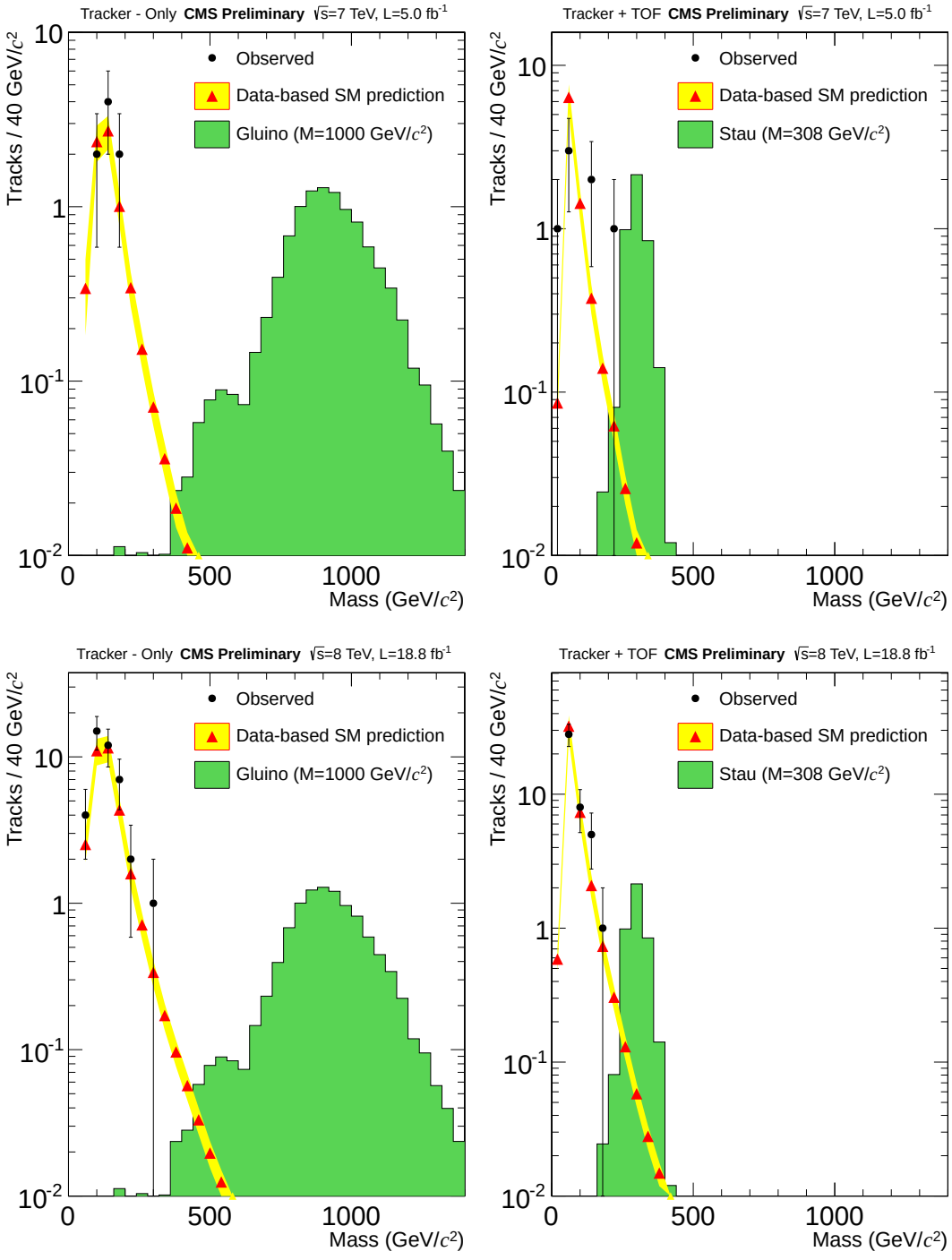

Figure 6: Observed and predicted mass spectra for candidates entering the tracker-only (left column) or tracker+TOF (right column) signal region for the tight selection. The expected distribution for a representative signal is shown in green. The top row is for $\sqrt{s} = 7\,\text{TeV}$, while the bottom row is for $\sqrt{s} = 8\,\text{TeV}$.

Table 1: Results of the final selections for predicted background and observed number of events. Uncertainties are statistical and systematic.

	Selection criteria				Numbers of events $\sqrt{s} = 7$ TeV		$\sqrt{s} = 8$ TeV	
	p_T (GeV/c)	$I_{as}^{(\prime)}$	$1/\beta$	Mass (GeV/c^2)	Pred.	Obs.	Pred.	Obs.
tracker-only	> 70	> 0.4	-	> 0	7.1 ± 1.5	8	32.5 ± 6.5	41
				> 100	6.0 ± 1.3	7	26.0 ± 5.2	29
				> 200	0.65 ± 0.14	0	3.1 ± 0.6	3
				> 300	0.11 ± 0.02	0	0.55 ± 0.11	1
				> 400	0.030 ± 0.006	0	0.15 ± 0.03	0
tracker+TOF	> 70	> 0.125	> 1.225	> 0	8.5 ± 1.7	7	43.5 ± 8.7	42
				> 100	1.0 ± 0.2	3	5.6 ± 1.1	7
				> 200	0.11 ± 0.02	1	0.56 ± 0.11	0
				> 300	0.020 ± 0.004	0	0.090 ± 0.02	0
muon-only	> 230	-	> 1.40	-	$-$	$-$	5.6 ± 2.9	3
$\lvert Q\rvert > 1e$	-	> 0.500	> 1.200	-	0.15 ± 0.04	0	0.52 ± 0.11	1
$\lvert Q\rvert < 1e$	> 125	> 0.275	-	-	0.12 ± 0.07	0	0.99 ± 0.24	0

6 Systematic Uncertainties

The sources of systematic uncertainty include those related to the integrated luminosity, the background prediction, and the signal efficiency. The uncertainty on the integrated luminosity is 2.2% (4.4%) at $\sqrt{s} = 7(8)$ TeV [54, 55]. The uncertainties on the background predictions are described in Sec. 5.

The signal efficiency is obtained from Monte Carlo simulations of the various signals processed through the full detector simulation (Sec. 2). Systematic uncertainties on the final results are dominated by uncertainties on the differences between the simulation and data. The relevant differences are discussed below. Uncertainties that vary between samples and masses are given by the range of values, other uncertainties are constant.

The trigger efficiency is dominated by the muon triggers for all the analyses except the charge-suppressed samples. The uncertainty on the muon trigger efficiency arises from several effects. A difference of up to 5% between data and MC has been observed [53]. For slow moving particles, the effect of timing synchronization of the muon system is tested by shifting the arrival times in MC by the synchronization observed in data resulting in an efficiency change of 2%(4%) for $\sqrt{s} = 7(8)$ TeV. For the $|Q| < 1e$ samples, an additional uncertainty arises from the possibility of losing hits due to their ionization in the muon system being closer to the hit threshold. The uncertainty on the gains in the muon system is evaluated by shifting the gain by 25% yielding an efficiency change of 15%(3%) for $|Q| = e/3(2e/3)$ samples. The uncertainty on the $E_{\mathrm{T}}^{\mathrm{miss}}$ trigger efficiency is found by varying the MC HLT jets by the jet energy scale uncertainties. The $E_{\mathrm{T}}^{\mathrm{miss}}$ uncertainty for $\sqrt{s} = 7$ TeV samples is found to be less than 2% for all samples except the charged suppressed where it is found to be $< 5\%$. For $\sqrt{s} = 8$ TeV samples it is less than 1% for all samples.

Energy loss in the silicon tracker is important for all the analyses except for the muon-only analysis. Low momentum protons are used to quantify the agreement between the observed

and simulated distributions for I_h and I_{as}. The dE/dx distributions of signal samples are varied by the observed differences in order to determine the systematic uncertainty. Because the fractionally charged analysis is also sensitive to changes to the number of hits on the track, track reconstruction is also performed after shifting dE/dx. The uncertainty on the signal acceptance varies by less than 24% for the $|Q| = 1e$ samples, being less than 10% for all masses above 200 GeV/c^2. For the $|Q| < 1e$ samples, the effect of the dE/dx shift and the track reconstruction combined is 25%(<10%) for $|Q| = e/3(2e/3)$. The $|Q| > 1e$ samples have sufficient separation of the signal from the final I_{as} selection that the dE/dx shift is negligible.

Decays of Z bosons to muons are used to test the MC simulation of $1/\beta$ by comparing to data. In 7 TeV data a disagreement is observed of 0.02 in the CSC system and 0.003 in the DT system on the $1/\beta$ measurement. For 8 TeV data a disagreement of 0.005 is found for both systems. The uncertainty on the signal acceptance is found to be 0–15% by shifting $1/\beta$ by these amounts. The uncertainty is generally less than 7% except for the high charge/low mass samples in the multiply charged analysis.

As in Ref. [25], the uncertainties on the efficiencies for muon reconstruction [53] and track reconstruction [56] are less than 2% each. The track momentum uncertainty is determined by shifting $1/p_T$ of muon system tracks for the muon-only analysis by 10% [53]. For all other analyses the momentum from the inner track is shifted as in Ref. [25]. The uncertainty is found to be <5% for all but the $|Q| < 1e$ samples, low mass $|Q| > 1e$ samples and the muon-only analysis where the uncertainty is less than 10%.

The uncertainty on the number of pile-up events is evaluated by varying by 5-6% the minimum bias cross section used to calculate the weights applied to signal events in order to reproduce the pile-up observed in data. This results in uncertainties due to pile-up of less than 4%.

The uncertainty on the amount of material in the detector simulation results in an uncertainty in the signal trigger and reconstruction efficiency, particularly for the $|Q| > 1e$ samples. This is evaluated by increasing the amount of material in the hadronic calorimeter by a conservative 5% [57]. The change in signal efficiency is $\leq 1\%$ for most samples, but $\sim$20% for the $|Q| > 1e$ samples.

The total systematic uncertainty on the signal efficiency for the tracker-only analysis is less than 30% and is less than 11% for all of the gluino and stop samples. For the tracker+TOF analysis it is less than 15% for all but the $|Q| = 2e/3$ sample where the uncertainty ranges from 15–31% being larger at low masses. The muon-only analysis has a signal uncertainty in the range of 7–13%. The multiply charged analysis has a signal uncertainty in the range of 21–29% for $|Q| > 1e$ samples and 7–13% for $|Q| = 1e$ samples with both being larger at low masses. The fractionally charged analysis has a signal uncertainty of 31% and 12% for $|Q| = 1e/3$ and $2e/3$ samples, respectively.

Table 2 summarizes the systematic uncertainties for the various analyses.

7 Results

No significant excess of events is observed over the predicted background. The largest excess for any of the selections shown in Table 1 has a significance of 1.3 one–sided Gaussian standard deviations. Cross section limits are placed at 95% confidence level (C.L.) for both $\sqrt{s} = 7$ TeV and 8 TeV using a CLs approach [58] where p-values are computed with a profile likelihood technique [59] that uses a lognormal model [60, 61] for the nuisance parameters. The latter are the integrated luminosity, the signal acceptance and the expected background in the signal

Table 2: Systematic uncertainties for the various HSCP searches. All values are relative uncertainties.

	$\|Q\| < 1e$	tracker-only	tracker+TOF	$\|Q\| > 1e$	muon-only
Signal acceptance	$< 31\%$	$< 32\%$	$< 31\%$	$< 29\%$	$< 13\%$
Expected collision background	20%	20%	20%	20%	20%
Expected cosmic background	50%	-	-	-	80%
Integrated luminosity	2.2%(4.4%) for $\sqrt{s} = 7(8)$ TeV				

region. For the combined dataset the limits are instead placed on the signal strength ($\mu = \sigma/\sigma_{th}$). Limits on the signal strength using only the 8 TeV dataset for the muon-only analysis are also presented. The observed limits are shown in Figs 7, 8 and 9 for all the analyses along with the theoretical predictions. For the gluino and stop pair production, the theoretical cross sections are computed at NLO+NLL [44–47] using PROSPINO [62] with CTEQ6.6M PDFs [63]. The uncertainty bands on the theoretical cross sections include the PDF uncertainty as well as the μ and α_s scale uncertainties. Mass limits are obtained from the intersection of the observed limit and the central value of the theoretical cross section. For the combined result, the mass limit is the point where the ratio crosses one.

From the final results, 95% C.L. limits on the production cross section are shown in Tables 3, 4, 5, and 6 for gluino, stop, stau, and Drell-Yan signals, respectively. The limits are determined from the numbers of events passing all final criteria (including the mass criteria for the tracker-only and tracker+TOF analyses). Figure 7 shows the limits as a function of mass for the tracker-only and tracker+TOF analyses. The tracker-only analysis excludes $f = 0.1$ gluino masses below 1322 and 1233 GeV/c^2 for the cloud interaction model and charge suppression model, respectively. Stop masses below 933(818) GeV/c^2 are excluded for the cloud (charge suppression) models. In addition, the tracker+TOF analysis excludes $\tilde{\tau}_1$ masses below 435(339) GeV/c^2 for the GMSB (pair production) model. Drell-Yan signals with $|Q| = 2e/3$ and $|Q| = 1e$ are excluded below 220 and 574 GeV/c^2, respectively.

The limits from the muon-only analysis for the gluino with various hadronization fractions, f, and the stop are shown in Fig. 8. The muon-only analysis excludes gluino masses below 1258(1283) GeV/c^2 for $f = 1.0(0.5)$.

Figure 9 shows the limits applied to the Drell-Yan production model for both the fractionally charged and multiply charged analyses. The fractionally charged analysis excludes masses below 200 and 480 GeV/c^2 for $|Q| = 1e/3$ and $|Q| = 2e/3$, respectively. The multiply charged analysis excludes masses below 517, 685, 752, 793, and 796 GeV/c^2 for $|Q| = 1e$, $2e$, $3e$, $4e$, and $5e$, respectively.

The mass limits for various signals and electric charges are shown in Fig 10 and are compared with previously published results. The mass limit obtained with the multiply charged analysis for Drell-Yan like production of particles with non unit charge in the range $e < |Q| < 5e$ can be parametrized as $M^{lower}_{95\%C.L.}(Q) = 404.9 + 154.6|Q| - 14.8Q^2$ GeV/c^2. The signal acceptance changes drastically between $|Q| = e/3, 2e/3$ and e and does not provide a reliable parametrization for $|Q| \leq e$ particles.

The mass limits obtained for the reanalyzed $\sqrt{s} = 7$ TeV dataset are similar to the previously published CMS results except for the GMSB and pair produced stau models where the mass limits are slightly worse. This is a consequence of having a common selection for all mass

Table 3: Signal efficiency (Eff.), expected (Exp.) and observed (Obs.) cross section limits for Gluino signals at $\sqrt{s} = 7$ TeV and 8 TeV as well as the ratio of the cross section limit to the theoretical value for the combination. The limit on the ratio for the muon-only analysis uses only $\sqrt{s} = 8$ TeV data.

Mass	M cut	σ (pb) ($\sqrt{s} = 7$ TeV)			σ (pb) ($\sqrt{s} = 8$ TeV)			σ/σ_{th} (7+8 TeV)	
(GeV/c^2)	(GeV/c^2)	Exp.	Obs.	Eff.	Exp.	Obs.	Eff.	Exp.	Obs.
Gluino ($f = 0.1$) particles with the tracker-only analysis									
300	> 100	0.0046	0.0068	0.15	0.0052	0.0055	0.15	3.7×10^{-5}	4.6×10^{-5}
700	> 370	0.0028	0.0030	0.19	7.7×10^{-4}	8.2×10^{-4}	0.19	0.0016	0.0017
1100	> 540	0.0039	0.0039	0.14	0.0011	0.0011	0.14	0.098	0.10
1500	> 530	0.0088	0.0081	0.07	0.0021	0.0022	0.07	5.0	5.4
Gluino ch. suppr. ($f = 0.1$) particles with the tracker-only analysis									
300	> 130	0.035	0.036	0.05	0.013	0.013	0.05	1.1×10^{-4}	1.2×10^{-4}
700	> 340	0.012	0.013	0.08	0.0021	0.0020	0.08	0.0044	0.0044
1100	> 410	0.018	0.019	0.06	0.0025	0.0026	0.06	0.24	0.24
1500	> 340	0.034	0.035	0.04	0.0045	0.0046	0.04	11	11
Gluino ($f = 0.5$) particles with the muon-only analysis									
300	-	-	-	-	0.0056	0.0065	0.06	5.5×10^{-5}	6.3×10^{-5}
700	-	-	-	-	0.0027	0.0022	0.12	0.0063	0.0053
1100	-	-	-	-	0.0025	0.0021	0.13	0.25	0.21
1500	-	-	-	-	0.0030	0.0025	0.11	7.6	6.4
Gluino ($f = 1.0$) particles with the muon-only analysis									
300	-	-	-	-	0.0066	0.0077	0.05	6.4×10^{-5}	7.4×10^{-5}
700	-	-	-	-	0.0032	0.0027	0.10	0.0076	0.0064
1100	-	-	-	-	0.0030	0.0025	0.11	0.30	0.25
1500	-	-	-	-	0.0038	0.0031	0.09	9.7	7.9

Table 4: Signal efficiency (Eff.), expected (Exp.) and observed (Obs.) cross section limits for Stop signals at $\sqrt{s} = 7$ TeV and 8 TeV as well as the ratio of the cross section limit to the theoretical value for the combination.

Mass	M cut	σ (pb) ($\sqrt{s} = 7$ TeV)			σ (pb) ($\sqrt{s} = 8$ TeV)			σ/σ_{th} (7+8 TeV)	
(GeV/c^2)	(GeV/c^2)	Exp.	Obs.	Eff.	Exp.	Obs.	Eff.	Exp.	Obs.
Stop particles with the tracker-only analysis									
200	> 0	0.0080	0.0087	0.18	0.0051	0.0051	0.18	2.6×10^{-4}	3.0×10^{-4}
500	> 120	0.0024	0.0024	0.23	0.0028	0.0034	0.23	0.022	0.026
800	> 330	0.0020	0.0021	0.22	7.2×10^{-4}	7.3×10^{-4}	0.22	0.21	0.22
Stop ch. suppr. particles with the tracker-only analysis									
200	> 0	0.063	0.075	0.05	0.018	0.026	0.05	0.0011	0.0014
500	> 120	0.0086	0.0089	0.10	0.0068	0.0081	0.10	0.062	0.070
800	> 270	0.0071	0.0076	0.10	0.0019	0.0023	0.10	0.61	0.74

points and models contrary to what was done in Ref. [25] where the selection was optimized separately for each mass point and model. The mass limit for $|Q| < 1e$ samples are significantly improved with respect to Ref. [24] thanks to a different analysis approach and to the use of the I'_{as} likelihood discriminator that maximally exploits all the dE/dx information associated to a track.

Table 5: Signal efficiency (Eff.), expected (Exp.) and observed (Obs.) cross section limits for Stau signals at $\sqrt{s} = 7$ TeV and 8 TeV as well as the ratio of the cross section limit to the theoretical value for the combination.

Mass (GeV/c^2)	M cut (GeV/c^2)	σ (pb) ($\sqrt{s} = 7$ TeV) Exp.	Obs.	Eff.	σ (pb) ($\sqrt{s} = 8$ TeV) Exp.	Obs.	Eff.	σ/σ_{th} (7+8 TeV) Exp.	Obs.
GMSB stau particles with the tracker+TOF analysis									
126	> 40	0.0046	0.0035	0.25	0.0042	0.0042	0.25	0.0075	0.0064
308	> 190	9.3×10^{-4}	0.0015	0.56	2.9×10^{-4}	2.9×10^{-4}	0.56	0.16	0.23
494	> 330	7.9×10^{-4}	7.9×10^{-4}	0.66	2.3×10^{-4}	2.4×10^{-4}	0.66	1.9	1.9
Pair prod. stau particles with the tracker+TOF analysis									
126	> 40	0.0056	0.0047	0.24	0.0044	0.0043	0.24	0.18	0.15
308	> 190	0.0011	0.0017	0.46	3.6×10^{-4}	3.4×10^{-4}	0.46	0.62	0.62
494	> 330	8.5×10^{-4}	8.6×10^{-4}	0.61	2.5×10^{-4}	2.7×10^{-4}	0.61	4.7	4.9

Table 6: Signal efficiency (Eff.), expected (Exp.) and observed (Obs.) cross section limits for Drell-Yan models of various charge at $\sqrt{s} = 7$ TeV and 8 TeV as well as the ratio of the cross section limit to the theoretical value for the combination.

Mass (GeV/c^2)	M cut (GeV/c^2)	σ (pb) ($\sqrt{s} = 7$ TeV) Exp.	Obs.	Eff.	σ (pb) ($\sqrt{s} = 8$ TeV) Exp.	Obs.	Eff.	σ/σ_{th} (7+8 TeV) Exp.	Obs.
Drell–Yan $\lvert Q\rvert = 1e/3$ particles with the $\lvert Q\rvert < 1$ analysis									
100	-	0.019	0.022	0.03	0.016	0.014	0.01	0.19	0.17
200	-	0.0094	0.011	0.06	0.0066	0.0058	0.03	1.2	0.99
400	-	0.0058	0.0066	0.10	0.0041	0.0035	0.05	15	13
Drell–Yan $\lvert Q\rvert = 2e/3$ particles with the $\lvert Q\rvert < 1$ analysis									
200	-	7.0×10^{-4}	7.6×10^{-4}	0.81	2.7×10^{-4}	2.4×10^{-4}	0.68	0.014	0.012
400	-	8.3×10^{-4}	9.0×10^{-4}	0.68	3.3×10^{-4}	3.4×10^{-4}	0.56	0.35	0.31
600	-	0.0012	0.0013	0.49	5.2×10^{-4}	5.3×10^{-4}	0.35	4.8	4.2
Drell–Yan $\lvert Q\rvert = 1e$ particles with the tracker+TOF analysis									
200	> 120	0.0015	0.0036	0.41	7.7×10^{-4}	0.0013	0.36	0.019	0.04
500	> 340	9.8×10^{-4}	0.001	0.60	2.8×10^{-4}	2.9×10^{-4}	0.56	0.41	0.44
800	> 530	0.001	0.001	0.58	3.0×10^{-4}	3.1×10^{-4}	0.52	7.5	8.1
Drell–Yan $\lvert Q\rvert = 2e$ particles with the $\lvert Q\rvert > 1$ analysis									
200	-	0.0016	0.0016	0.36	5.0×10^{-4}	7.3×10^{-4}	0.33	0.0028	0.004
500	-	0.00098	0.001	0.59	2.9×10^{-4}	4.2×10^{-4}	0.56	0.11	0.15
800	-	0.0011	0.0011	0.55	2.9×10^{-4}	4.2×10^{-4}	0.56	1.9	2.5
Drell–Yan $\lvert Q\rvert = 3e$ particles with the $\lvert Q\rvert > 1$ analysis									
200	-	0.0031	0.0034	0.18	9.0×10^{-4}	0.0013	0.18	0.0023	0.0032
500	-	0.0012	0.0013	0.47	3.5×10^{-4}	5.1×10^{-4}	0.46	0.059	0.083
800	-	0.0012	0.0013	0.47	3.3×10^{-4}	4.8×10^{-4}	0.49	0.99	1.4
Drell–Yan $\lvert Q\rvert = 4e$ particles with the $\lvert Q\rvert > 1$ analysis									
200	-	0.0082	0.0088	0.07	0.0021	0.003	0.08	0.0031	0.0045
500	-	0.0018	0.002	0.31	5.1×10^{-4}	7.4×10^{-4}	0.32	0.048	0.068
800	-	0.0017	0.0018	0.34	4.5×10^{-4}	6.4×10^{-4}	0.37	0.75	1
Drell–Yan $\lvert Q\rvert = 5e$ particles with the $\lvert Q\rvert > 1$ analysis									
200	-	0.03	0.032	0.02	0.0066	0.0096	0.02	0.0064	0.0092
500	-	0.0035	0.0037	0.16	8.6×10^{-4}	0.0013	0.19	0.052	0.073
800	-	0.0026	0.0027	0.22	6.6×10^{-4}	0.00096	0.24	0.71	1

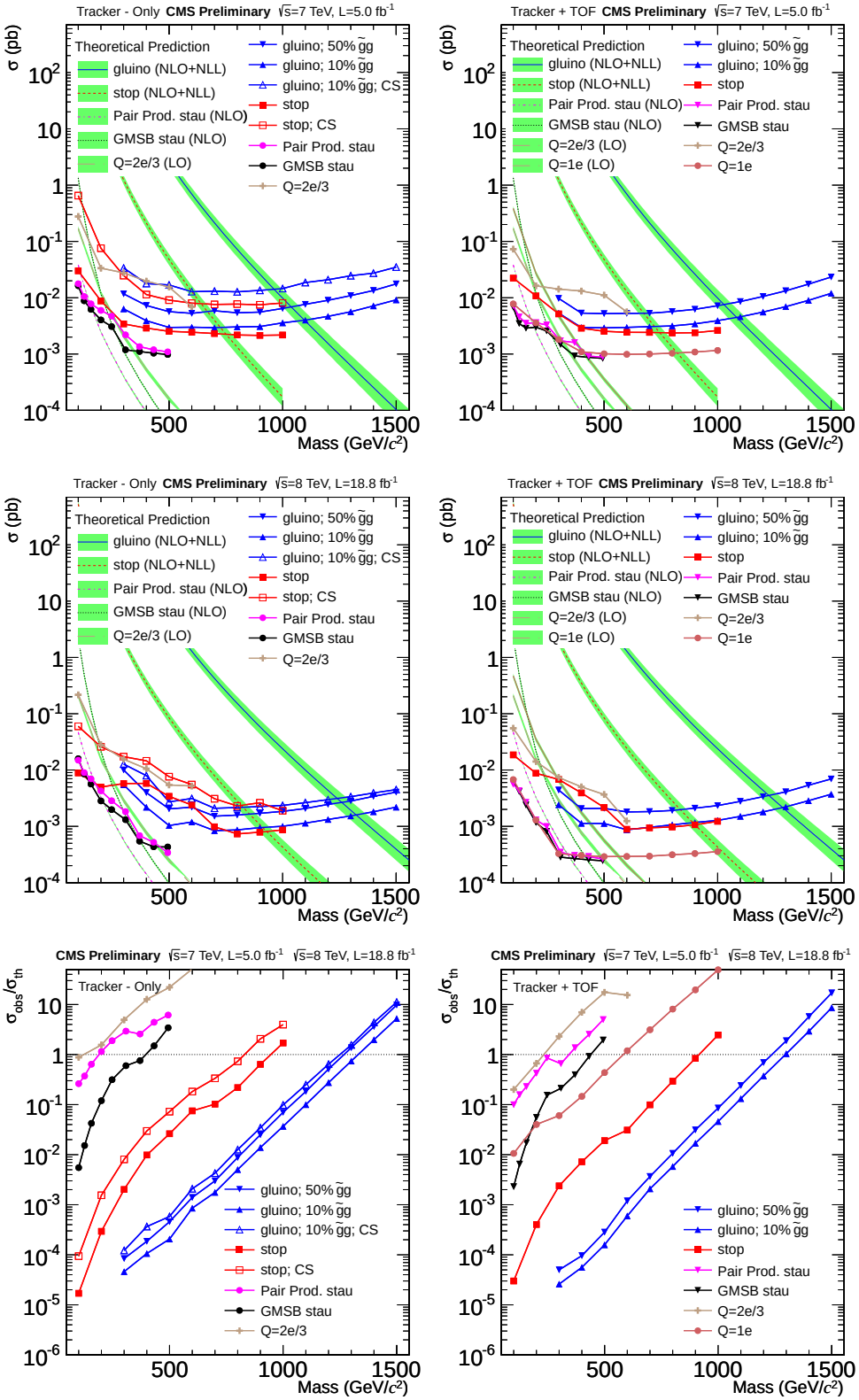

Figure 7: Cross section upper limits at 95% C.L. on various signal models for the tracker-only analysis (left column) and tracker+TOF analysis (right column). The top row is for the 2011 data ($\sqrt{s} = 7$ TeV), the middle row is for the 2012 data ($\sqrt{s} = 8$ TeV), the bottom row shows the ratio of the limit to the theoretical value for the combined 2011 and 2012 dataset. In the legend, 'CS' stands for charged suppressed interaction model.

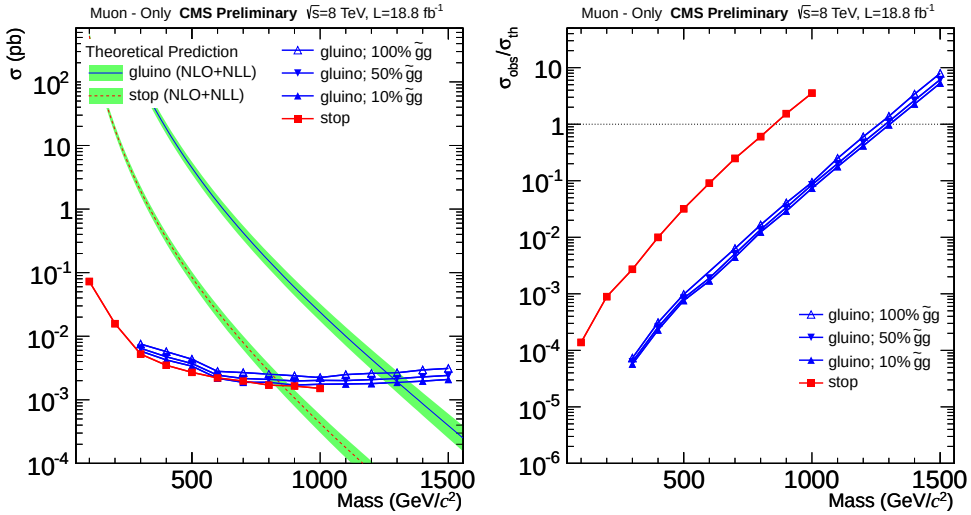

Figure 8: Left: Cross section upper limits at 95% C.L. on various signal models for the muon-only analysis for the 2012 ($\sqrt{s} = 8$ TeV) dataset. Right: Limits on the signal strength ($\mu = \sigma/\sigma_{th}$) for the 2012 ($\sqrt{s} = 8$ TeV) dataset.

8 Conclusions

A wide ranging, multi-prong search for heavy, stable, charged particles is presented with CMS data at $\sqrt{s} = 7$ and 8 TeV. Five complementary, and sometimes overlapping, analyses are performed: a search with only the inner tracker; a search with both the inner tracker and the muon system; a search with only the muon system; a search for low ionizing tracks; and a search for tracks with very large ionization energy loss as expected for particles with $|Q| = 2 - 5e$. No significant excess is observed. Mass limits for gluinos, stops, staus, fractionally charged particles, and multiply charged particles are given. The models for R-hadron-like HSCPs include a varying fraction of $\tilde{g}-$gluon production and two different interaction models producing a variety of exotic experimental signatures. The multiply charged analysis gives the first CMS limits on the production of long lived particles with $|Q| = 2 - 5e$. The other limits, ranging up to 1322 GeV/c^2 for gluinos, are the most restrictive to date eclipsing previous limits from the LHC.

References

[1] M. Drees and X. Tata, "Signals for heavy exotics at hadron colliders and supercolliders", *Phys. Lett.* **B 252** (1990) 695, doi:10.1016/0370-2693(90)90508-4.

[2] M. Fairbairn et al., "Stable massive particles at colliders", *Phys. Rept.* **438** (2007) 1, doi:10.1016/j.physrep.2006.10.002, arXiv:hep-ph/0611040.

[3] C. W. Bauer et al., "Supermodels for early LHC", *Phys. Lett.* **B 690** (2010) 280–288, doi:10.1016/j.physletb.2010.05.032, arXiv:0909.5213.

[4] A. Kusenko and M. E. Shaposhnikov, "Supersymmetric Q-balls as dark matter", *Phys. Lett.* **B 418** (1998) 46–54, doi:10.1016/S0370-2693(97)01375-0, arXiv:hep-ph/9709492.

[5] B. Koch, M. Bleicher, and H. Stoecker, "Black holes at LHC?", *J. Phys.* **G 34** (2007) S535–542, doi:10.1088/0954-3899/34/8/S44, arXiv:hep-ph/0702187.

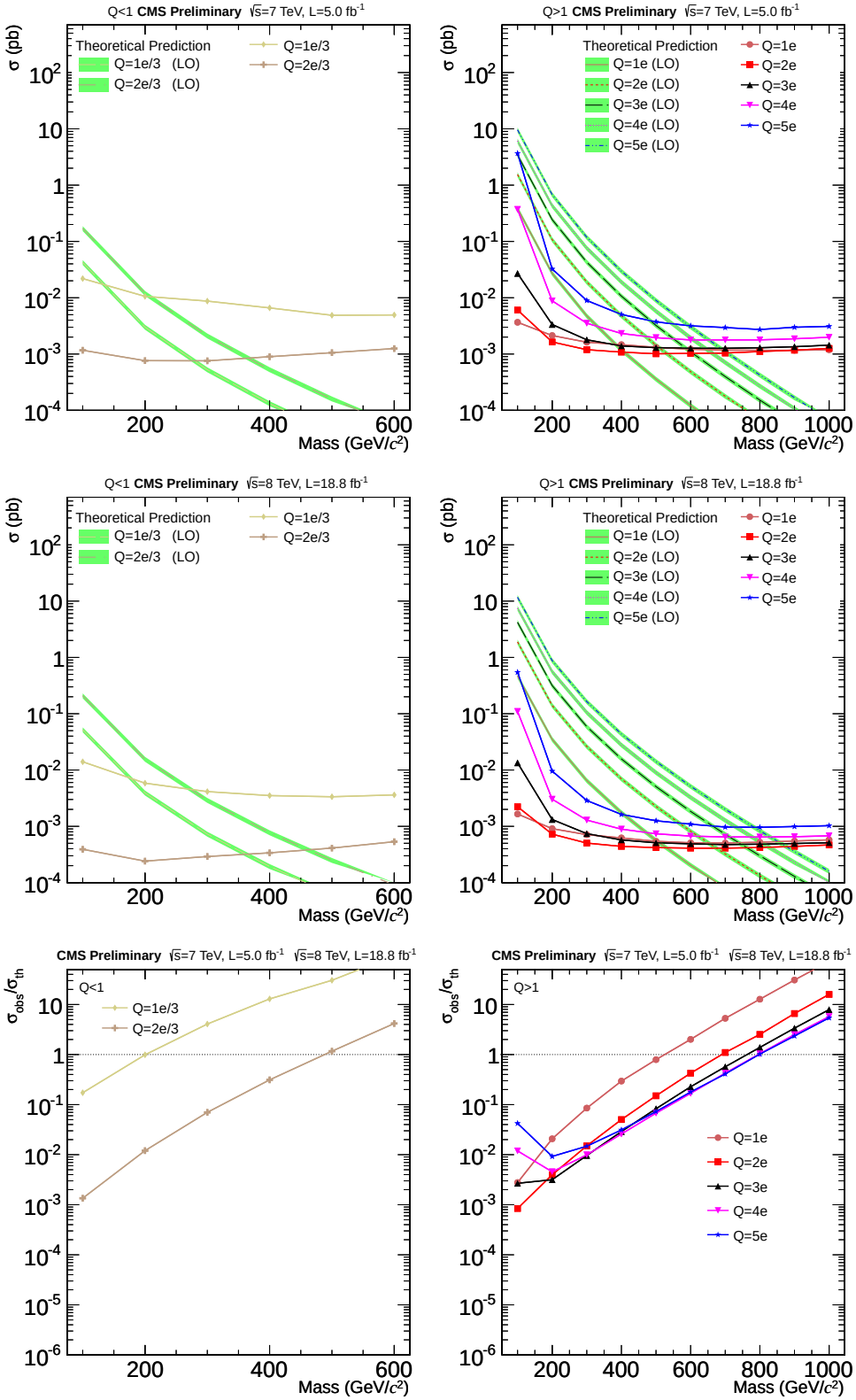

Figure 9: Cross section upper limits at 95% C.L. on various signal models for the fractionally charged analysis (left column) and multiply charged analysis (right column). The top row is for the 2011 data ($\sqrt{s} = 7\,\text{TeV}$), the middle row is for the 2012 data ($\sqrt{s} = 8\,\text{TeV}$), the bottom row shows the ratio of the limit to the theoretical value for the combined 2011 and 2012 dataset.

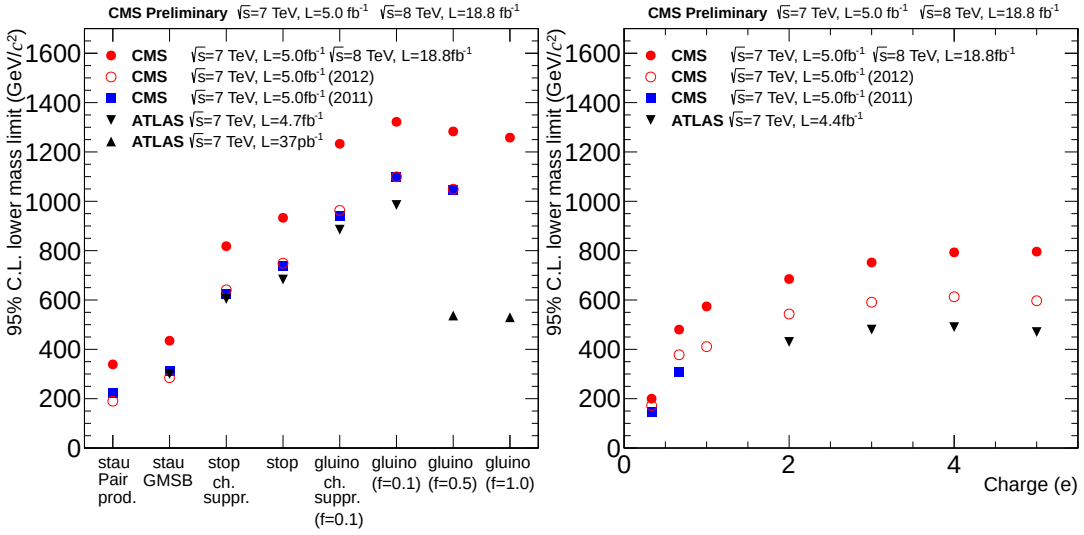

Figure 10: Obtained mass lower limits at 95% C.L. on various models compared with previously published results [18–25]. Left: The model type is defined by the X-axis. Right: Mass limits for Drell-Yan like production versus electric charge.

[6] J. S. Schwinger, "Magnetic charge and quantum field theory", *Phys. Rev.* **144** (1966) 1087–1093, doi:10.1103/PhysRev.144.1087.

[7] D. Fargion, M. Khlopov, and C. A. Stephan, "Cold dark matter by heavy double charged leptons?", *Class. Quant. Grav.* **23** (2006) 7305–7354, doi:10.1088/0264-9381/23/24/008, arXiv:astro-ph/0511789.

[8] Particle Data Group Collaboration, "Review of Particle Physics (RPP)", *Phys. Rev.* **D 86** (2012) 010001, doi:10.1103/PhysRevD.86.010001.

[9] ALEPH Collaboration, "Search for pair production of longlived heavy charged particles in e^+e^- annihilation", *Phys. Lett.* **B 405** (1997) 379–388, doi:10.1016/S0370-2693(97)00715-6, arXiv:hep-ex/9706013.

[10] DELPHI Collaboration, "Search for heavy stable and longlived particles in e^+e^- collisions at $\sqrt{s} = 189\,\text{GeV}$", *Phys. Lett.* **B 478** (2000) 65–72, doi:10.1016/S0370-2693(00)00265-3, arXiv:hep-ex/0103038.

[11] L3 Collaboration, "Search for heavy neutral and charged leptons in e^+e^- annihilation at LEP", *Phys. Lett.* **B 517** (2001) 75–85, doi:10.1016/S0370-2693(01)01005-X, arXiv:hep-ex/0107015.

[12] OPAL Collaboration, "Search for stable and longlived massive charged particles in e^+e^- collisions at $\sqrt{s} = 130$ GeV to 209GeV", *Phys. Lett.* **B 572** (2003) 8–20, doi:10.1016/S0370-2693(03)00639-7, arXiv:hep-ex/0305031.

[13] H1 Collaboration, "Measurement of anti-deuteron photoproduction and a search for heavy stable charged particles at HERA", *Eur. Phys. J.* **C 36** (2004) 413–423, doi:10.1140/epjc/s2004-01894-1, arXiv:hep-ex/0403056.

[14] CDF Collaboration, "Search for long-lived massive charged particles in 1.96 TeV $\bar{p}p$ collisions", *Phys. Rev. Lett.* **103** (2009) 021802, doi:10.1103/PhysRevLett.103.021802, arXiv:0902.1266.

[15] D0 Collaboration, "Search for long-lived charged massive particles with the D0 detector", *Phys. Rev. Lett.* **102** (2009) 161802, doi:10.1103/PhysRevLett.102.161802, arXiv:0809.4472.

[16] D0 Collaboration, "A search for charged massive long-lived particles", *Phys. Rev. Lett.* **108** (2012) 121802, doi:10.1103/PhysRevLett.108.121802, arXiv:1110.3302.

[17] D0 Collaboration, "Search for charged massive long-lived particles at $\sqrt{s} = 1.96$ TeV", arXiv:1211.2466.

[18] ATLAS Collaboration, "Search for heavy long-lived charged particles with the ATLAS detector in pp collisions at $\sqrt{s} = 7$ TeV", *Phys. Lett.* **B 703** (2011) 428–446, doi:10.1016/j.physletb.2011.08.042, arXiv:1106.4495.

[19] ATLAS Collaboration, "Search for stable hadronising squarks and gluinos with the ATLAS experiment at the LHC", *Phys. Lett.* **B 701** (2011) 1–19, doi:10.1016/j.physletb.2011.05.010, arXiv:1103.1984.

[20] ATLAS Collaboration, "Search for massive long-lived highly ionising particles with the ATLAS detector at the LHC", *Phys. Lett.* **B 698** (2011) 353–370, doi:10.1016/j.physletb.2011.03.033, arXiv:1102.0459.

[21] ATLAS Collaboration, "Searches for heavy long-lived sleptons and R-Hadrons with the ATLAS detector in pp collisions at $\sqrt{s} = 7$ TeV", arXiv:1211.1597.

[22] ATLAS Collaboration, "Search for long-lived, multi-charged particles in pp collisions at sqrt(s)=7 TeV using the ATLAS detector", arXiv:1301.5272.

[23] CMS Collaboration, "Search for heavy stable charged particles in pp collisions at $\sqrt{s} = 7$ TeV", *JHEP* **03** (2011) 024, doi:10.1007/JHEP03(2011)024, arXiv:1101.1645.

[24] CMS Collaboration, "Search for fractionally charged particles in pp collisions at $\sqrt{s} = 7$ TeV", *Phys. Rev. Lett.* (2012) arXiv:1210.2311.

[25] CMS Collaboration, "Search for heavy long-lived charged particles in pp collisions at $\sqrt{s} = 7$ TeV", *Phys. Lett.* **B 713** (2012) 408–433, doi:10.1016/j.physletb.2012.06.023, arXiv:1205.0272.

[26] C. F. Berger et al., "Supersymmetry without prejudice", *JHEP* **0902** (2009) 023, doi:10.1088/1126-6708/2009/02/023, arXiv:0812.0980.

[27] M. W. Cahill-Rowley et al., "More energy, more searches, but the pMSSM lives on", arXiv:1211.1981.

[28] A. C. Kraan, "Interactions of heavy stable hadronizing particles", *Eur. Phys. J. C* **37** (2004) 91–104, doi:10.1140/epjc/s2004-01997-7, arXiv:hep-ex/0404001.

[29] R. Mackeprang and A. Rizzi, "Interactions of coloured heavy stable particles in matter", *Eur. Phys. J. C* **50** (2007) 353–362, doi:10.1140/epjc/s10052-007-0252-4, arXiv:hep-ph/0612161.

[30] R. Mackeprang and D. Milstead, "An updated description of heavy-hadron interactions in GEANT4", *Eur. Phys. J. C* **66** (2010) 493–501, doi:10.1140/epjc/s10052-010-1262-1, arXiv:0908.1868.

[31] S. Agostinelli et al., "GEANT4–a simulation toolkit", *Nucl. Instrum. Meth. A* **506** (2003) 250, doi:10.1016/S0168-9002(03)01368-8.

[32] J. Allison et al., "GEANT4 developments and applications", *IEEE Trans. Nucl. Sci.* **53** (2006) 270 – 278, doi:10.1109/TNS.2006.869826.

[33] J. Pumplin et al., "New generation of parton distributions with uncertainties from global QCD analysis", *JHEP* **0207** (2002) 012, arXiv:hep-ph/0201195.

[34] G. Giudice and R. Rattazzi, "Theories with gauge mediated supersymmetry breaking", *Phys. Rept.* **322** (1999) 419–499, doi:10.1016/S0370-1573(99)00042-3, arXiv:hep-ph/9801271.

[35] T. Sjöstrand, S. Mrenna, and P. Z. Skands, "PYTHIA 6.4 physics and manual", *JHEP* **05** (2006) 026, doi:10.1088/1126-6708/2006/05/026, arXiv:hep-ph/0603175.

[36] B. Allanach et al., "The Snowmass points and slopes: Benchmarks for SUSY searches", *Eur. Phys. J. C* **25** (2002) 113–123, doi:10.1007/s10052-002-0949-3, arXiv:hep-ph/0202233.

[37] W. Beenakker et al., "The production of charginos / neutralinos and sleptons at hadron colliders", *Phys. Rev. Lett.* **83** (1999) 3780–3783, doi:10.1103/PhysRevLett.100.029901,10.1103/PhysRevLett.83.3780, arXiv:hep-ph/9906298.

[38] T. Sjostrand, S. Mrenna, and P. Z. Skands, "A brief introduction to PYTHIA 8.1", *Comput. Phys. Commun.* **178** (2008) 852–867, doi:10.1016/j.cpc.2008.01.036, arXiv:0710.3820.

[39] N. Arkani-Hamed and S. Dimopoulos, "Supersymmetric unification without low energy supersymmetry and signatures for fine-tuning at the LHC", *JHEP* **06** (2005) 073, doi:10.1088/1126-6708/2005/06/073, arXiv:hep-th/0405159.

[40] G. Giudice and A. Romanino, "Split supersymmetry", *Nucl. Phys. B* **699** (2004) 65–89, doi:10.1016/j.nuclphysb.2004.11.048, arXiv:hep-ph/0406088.

[41] M. Kramer et al., "Supersymmetry production cross sections in pp collisions at $\sqrt{s} = 7$ TeV", arXiv:1206.2892.

[42] W. Beenakker et al., "Squark and gluino production at hadron colliders", *Nucl. Phys.* **B 492** (1997) 51–103, doi:10.1016/S0550-3213(97)00084-9, arXiv:hep-ph/9610490.

[43] W. Beenakker et al., "Stop production at hadron colliders", *Nucl. Phys.* **B 515** (1998) 3–14, doi:10.1016/S0550-3213(98)00014-5, arXiv:hep-ph/9710451.

[44] A. Kulesza and L. Motyka, "Threshold resummation for squark-antisquark and gluino-pair production at the LHC", *Phys. Rev. Lett.* **102** (2009) 111802, doi:10.1103/PhysRevLett.102.111802, arXiv:0807.2405.

[45] A. Kulesza and L. Motyka, "Soft gluon resummation for the production of gluino-gluino and squark-antisquark pairs at the LHC", *Phys. Rev.* **D 80** (2009) 095004, doi:10.1103/PhysRevD.80.095004, arXiv:0905.4749.

[46] W. Beenakker et al., "Soft-gluon resummation for squark and gluino hadroproduction", *JHEP* **0912** (2009) 041, doi:10.1088/1126-6708/2009/12/041, arXiv:0909.4418.

[47] W. Beenakker et al., "Supersymmetric top and bottom squark production at hadron colliders", *JHEP* **1008** (2010) 098, doi:10.1007/JHEP08(2010)098, arXiv:1006.4771.

[48] W. Beenakker et al., "Squark and gluino hadroproduction", *Int. J. Mod. Phys.* **A 26** (2011) 2637–2664, doi:10.1142/S0217751X11053560, arXiv:1105.1110.

[49] P. Langacker and G. Steigman, "Requiem for an FCHAMP? Fractionally CHArged, Massive Particle", *Phys. Rev.* **D84** (2011) 065040, doi:10.1103/PhysRevD.84.065040, arXiv:1107.3131.

[50] CMS Collaboration, "The CMS experiment at the CERN LHC", *JINST* **3** (2008) S08004, doi:10.1088/1748-0221/3/08/S08004.

[51] CMS Collaboration, "Jet performance in pp collisions at $\sqrt{s}$=7 TeV", CMS Physics Analysis Summary CMS-PAS-JME-10-003, CMS, (2010).

[52] CMS Collaboration, "Particle–flow event reconstruction in CMS and performance for jets, taus, and $E_{\mathrm{T}}^{\mathrm{miss}}$", CMS Physics Analysis Summary CMS-PAS-PFT-09-001, CERN, (2009).

[53] CMS Collaboration, "Performance of CMS muon reconstruction in pp collision events at $\sqrt{s}$ = 7 TeV", *JINST* **7** (2012) P10002, doi:10.1088/1748-0221/7/10/P10002, arXiv:1206.4071.

[54] CMS Collaboration, "CMS Luminosity Based on Pixel Cluster Counting - Summer 2012 Update", CMS Physics Analysis Summary CMS-PAS-LUM-12-001, (2012).

[55] CMS Collaboration, "Absolute Calibration of the Luminosity Measurement at CMS: Winter 2012 Update", CMS Physics Analysis Summary CMS-PAS-SMP-12-008, CMS, (2012).

[56] CMS Collaboration, "Measurement of tracking efficiency", CMS Physics Analysis Summary CMS-PAS-TRK-10-002, CMS, (2010).

[57] CMS Collaboration, "Precise Mapping of the Magnetic Field in the CMS Barrel Yoke using Cosmic Rays", *JINST* **5** (2010) T03021, doi:10.1088/1748-0221/5/03/T03021, arXiv:0910.5530.

[58] A. L. Read, "Modified frequentist analysis of search results (The CL(s) method)",.

[59] G. Cowan et al., "Asymptotic formulae for likelihood-based tests of new physics", *Eur.Phys.J.* **C71** (2011) 1554, doi:10.1140/epjc/s10052-011-1554-0, arXiv:1007.1727.

[60] W. T. Eadie et al., "Statistical methods in experimental physics". North Holland, Amsterdam, 1971.

[61] F. James, "Statistical methods in experimental physics". World Scientific, Singapore, 2006.

[62] W. Beenakker, R. Hopker, and M. Spira, "PROSPINO: A program for the PROduction of Supersymmetric Particles In Next-to-leading Order QCD", arXiv:hep-ph/9611232.

[63] P. M. Nadolsky et al., "Implications of CTEQ global analysis for collider observables", *Phys. Rev.* **D78** (2008) 013004, doi:10.1103/PhysRevD.78.013004, arXiv:0802.0007.